Real-Time Time-Dependent Nuclear-Electronic Orbital Approach: Dynamics Beyond the Born-Oppenheimer Approximation

Luning Zhao,[†] Zhen Tao,[‡] Fabijan Pavošević,[‡] Andrew Wildman,[†] Sharon Hammes-Schiffer,[*,‡] and Xiaosong Li[*,†]

†*Department of Chemistry, University of Washington, Seattle, Washington, 98195, USA*

‡*Department of Chemistry, Yale University, 225 Prospect Street, New Haven, Connecticut, 06520, USA*

E-mail: sharon.hammes-schiffer@yale.edu; xsli@uw.edu

Abstract

The quantum mechanical treatment of both electrons and nuclei is crucial in nonadiabatic dynamical processes such as proton-coupled electron transfer. The nuclear electronic orbital (NEO) method provides an elegant framework for including nuclear quantum effects beyond the Born-Oppenheimer approximation. To enable the study of nonequilibrium properties, we derive and implement a real-time NEO (RT-NEO) approach based on time-dependent Hatree-Fock or density functional theory, in which both the electronic and nuclear degrees of freedom are propagated in a time-dependent variational framework. Nuclear and electronic spectral features can be resolved from the time-dependent dipole moment computed using the RT-NEO method. The test cases show the dynamical interplay between the quantum nuclei and the electrons through vibronic coupling. Moreover, vibrational excitation in the RT-NEO approach is demonstrated by applying a resonant driving field, and electronic excitation is demonstrated by simulating excited state intramolecular proton transfer. This work shows that the RT-NEO approach is a promising tool to study nonadiabatic quantum dynamical processes within a time-dependent variational description for the coupled electronic and nuclear degrees of freedom.

Graphical TOC Entry

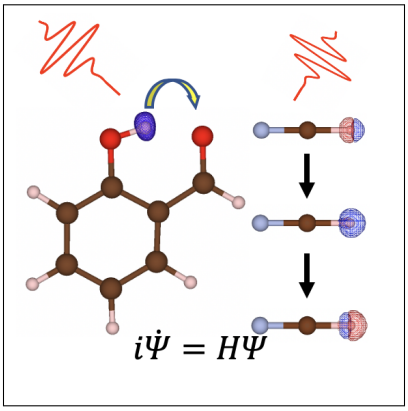

Keywords

American Chemical Society, LaTeX

First-principles simulation of the time evolution of a quantum system is a powerful tool to probe the underlying physical principles of ultrafast, nonequilibrium, and nonadiabatic chemical processes with spatial and temporal resolution unparalleled by most experiments. The exact non-relativistic quantum dynamics formally mandates treatment in the framework of the full time-dependent Schrödinger equation for the entire (electronic plus nuclear) system. This treatment represents a computationally prohibitive prospect for all but the smallest of molecules with a few active electrons.

Various approximations based on the nature of the chemical system of interest have been introduced with the aim of achieving reliable results at lower computational cost. The existing approaches for quantum dynamics rely heavily on semi-classical approximations, in which nuclei are treated as classical particles and/or electronic degrees of freedom are represented by a relatively small number of electronic potential energy surfaces. These methods include Ehrenfest dynamics,[1–6] surface hopping,[7–11] *ab initio* multiple spawning,[12–15] multiconfigurational time-dependent Hartree (MCTDH),[16,17] and Gaussian wave packet dynamics.[18,19] However, without treating nuclei fully quantum mechanically, effects such as quantized vibrational states, vibronic coupling, and nuclear tunneling would be difficult to describe, if not impossible. On the other hand, quantum dynamics of electronic degrees of freedom is needed when a molecular reaction is subject to a strong field perturbation or in the strong nonadiabatic regime where electronic adiabatic potential energy surfaces are no longer well-defined.

This Letter aims to introduce a full quantum description of coupled nuclear-electronic dynamics that follows the time-dependent variational principle and treats both electronic and specified nuclear degrees of freedom on equal footing. Such a computational framework will allow for quantum dynamical studies of proton-coupled electron transfer,[20,21] thermally activated singlet fission,[22,23] and quantum decoherence.[24,25] Obtaining fundamental knowledge of these processes could potentially aid the development of artificial photosynthesis,[26] light-harvesting materials,[27] and scalable quantum computers.[28]

A promising and computationally tractable approach is based on the multicomponent nuclear-electronic orbital (NEO) framework, which treats specified nuclei quantum mechanically on the same level as the electrons with molecular orbital techniques.[29–32] The NEO approach has been implemented in conjunction with methods widely used in electronic structure theory, such as Hartree-Fock (HF),[29] density functional theory (DFT),[32–34] perturbation theory,[35] coupled-cluster,[36,37] and multi-reference methods[29] to study coupled nuclear-electronic quantum effects in both ground and excited states.

Quantum mechanical solutions based on the time-independent Schrödinger equation within the NEO framework have been successfully applied to study proton delocalization in the ground state wavefunctions of small molecules.[29–33,36] Recently, the NEO approach has been extended to investigate both electronic and proton vibrational excited states with the linear response[38] and equation-of-motion[37] formalisms. While these methodological advances can provide stationary characteristics of combined electronic and protonic quantum mechanical systems, studies of nonequilibrium nonadiabatic processes require the solution of the time-dependent Schrödinger equation.

The dynamics of electrons and protons are determined by the time-dependent Schrödinger equation,

$$i\hbar\frac{\partial}{\partial t}\Psi_{\mathrm{NEO}}(\boldsymbol{x}^{\mathrm{e}},\boldsymbol{x}^{\mathrm{p}};t) = H(\boldsymbol{x}^{\mathrm{e}},\boldsymbol{x}^{\mathrm{p}};t)\Psi_{\mathrm{NEO}}(\boldsymbol{x}^{\mathrm{e}},\boldsymbol{x}^{\mathrm{p}};t) \tag{1}$$

in which $\boldsymbol{x}^{\mathrm{e}}$ and $\boldsymbol{x}^{\mathrm{p}}$ are the coordinates including both spatial and spin degrees of freedom for electrons and protons, respectively. For single-determinant methods, *e.g.*, HF and DFT, the wavefunction assumes the form of the following ansatz,

$$\Psi_{\mathrm{NEO}}(\boldsymbol{x}^{\mathrm{e}},\boldsymbol{x}^{\mathrm{p}};t) = \Phi^{\mathrm{e}}(\boldsymbol{x}^{\mathrm{e}};t)\Phi^{\mathrm{p}}(\boldsymbol{x}^{\mathrm{p}};t) \tag{2}$$

in which Φ^{e} and Φ^{p} are single Slater determinants for the electrons and protons.

By taking advantage of the product separable form of the wavefunction ansatz, Eq. (1) can be written as two coupled differential equations that describe the motions of the electrons

and protons:

$$
\begin{aligned}
i\hbar\frac{\partial}{\partial t}\boldsymbol{C}^{\mathrm{e}}(t) &= \boldsymbol{F}^{\mathrm{e}}(t)\boldsymbol{C}^{\mathrm{e}}(t) \\
i\hbar\frac{\partial}{\partial t}\boldsymbol{C}^{\mathrm{p}}(t) &= \boldsymbol{F}^{\mathrm{p}}(t)\boldsymbol{C}^{\mathrm{p}}(t)
\end{aligned}
\tag{3}
$$

where $\boldsymbol{C}^{\mathrm{e}}(t)$ and $\boldsymbol{C}^{\mathrm{p}}(t)$ are the time-dependent orbital coefficients for the electrons and protons, respectively. $\boldsymbol{P}$ is the one-particle density matrix and $\boldsymbol{F}$ is the Fock/Kohn-Sham matrix, both in the orthonormal atomic orbital basis. Note that we will use primed notations (*e.g.*, $\boldsymbol{F}'$ and $\boldsymbol{P}'$) for quantities in the non-orthogonal atomic orbital basis. In this work, the orthonormal basis is obtained with the Löwdin orthogonalization scheme.[39]

The Fock/Kohn-Sham matrices can be split into single- and multi-component contributions,

$$
\begin{aligned}
\boldsymbol{F}^{\mathrm{e}}(t) &= \boldsymbol{H}^{\mathrm{ee}}(t, \boldsymbol{P}^{\mathrm{e}}(t)) + \boldsymbol{H}^{\mathrm{ep}}(\boldsymbol{P}^{\mathrm{e}}(t), \boldsymbol{P}^{\mathrm{p}}(t)) \\
\boldsymbol{F}^{\mathrm{p}}(t) &= \boldsymbol{H}^{\mathrm{pp}}(t, \boldsymbol{P}^{\mathrm{p}}(t)) + \boldsymbol{H}^{\mathrm{pe}}(\boldsymbol{P}^{\mathrm{p}}(t), \boldsymbol{P}^{\mathrm{e}}(t))
\end{aligned}
\tag{4}
$$

The single-component contributions to the Fock/Kohn-Sham matrices are

$$
\begin{aligned}
\boldsymbol{H}^{\mathrm{ee}}(t, \boldsymbol{P}^{\mathrm{e}}(t)) &= \boldsymbol{H}^{\mathrm{e}}_{\mathrm{core}} + \boldsymbol{J}^{\mathrm{ee}}(\boldsymbol{P}^{\mathrm{e}}(t)) + \zeta\boldsymbol{K}^{\mathrm{ee}}(\boldsymbol{P}^{\mathrm{e}}(t)) + (1-\zeta)\boldsymbol{V}^{\mathrm{e}}_{xc}(\boldsymbol{P}^{\mathrm{e}}(t)) + \boldsymbol{V}^{\mathrm{e}}_{ext}(t) \\
\boldsymbol{H}^{\mathrm{pp}}(t, \boldsymbol{P}^{\mathrm{p}}(t)) &= \boldsymbol{H}^{\mathrm{p}}_{\mathrm{core}} + \boldsymbol{J}^{\mathrm{pp}}(\boldsymbol{P}^{\mathrm{p}}(t)) + \zeta\boldsymbol{K}^{\mathrm{pp}}(\boldsymbol{P}^{\mathrm{p}}(t)) + (1-\zeta)\boldsymbol{V}^{\mathrm{p}}_{xc}(\boldsymbol{P}^{\mathrm{p}}(t)) + \boldsymbol{V}^{\mathrm{p}}_{ext}(t)
\end{aligned}
\tag{5}
$$

in which $\boldsymbol{H}_{\mathrm{core}}$ is the core Hamiltonian that includes the kinetic energy and the interaction with the classical nuclei. $\boldsymbol{J}^{\mathrm{ee(pp)}}$ and $\boldsymbol{K}^{\mathrm{ee(pp)}}$ are the Coulomb and HF exchange matrices, respectively, between electrons (protons). $\boldsymbol{V}^{\mathrm{e}}_{xc}$ and $\boldsymbol{V}^{\mathrm{p}}_{xc}$ are the electron-electron and proton-proton exchange-correlation potentials. ζ is a parameter that converts the Fock matrix between HF ($\zeta = 1$) and DFT ($\zeta = 0$), and $\boldsymbol{V}_{ext}(t)$ is the time-dependent external potential such as an electric field. The multi-component contributions to the Fock matrices are given

by

$$\begin{aligned}
\boldsymbol{H}^{\mathrm{ep}}(\boldsymbol{P}^{\mathrm{e}}(t),\boldsymbol{P}^{\mathrm{p}}(t)) &= -\boldsymbol{J}^{\mathrm{ep}}(\boldsymbol{P}^{\mathrm{e}}(t),\boldsymbol{P}^{\mathrm{p}}(t)) + (1-\zeta)\boldsymbol{V}_c^{\mathrm{ep}}(\boldsymbol{P}^{\mathrm{e}}(t),\boldsymbol{P}^{\mathrm{p}}(t)) \\
\boldsymbol{H}^{\mathrm{pe}}(\boldsymbol{P}^{\mathrm{p}}(t),\boldsymbol{P}^{\mathrm{e}}(t)) &= -\boldsymbol{J}^{\mathrm{pe}}(\boldsymbol{P}^{\mathrm{p}}(t),\boldsymbol{P}^{\mathrm{e}}(t)) + (1-\zeta)\boldsymbol{V}_c^{\mathrm{pe}}(\boldsymbol{P}^{\mathrm{p}}(t),\boldsymbol{P}^{\mathrm{e}}(t))
\end{aligned} \tag{6}$$

where $\boldsymbol{J}^{\mathrm{ep}}(\boldsymbol{J}^{\mathrm{pe}})$ is the classical Coulomb interaction between electrons and protons, and $\boldsymbol{V}_c^{\mathrm{ep}}(\boldsymbol{V}_c^{\mathrm{pe}})$ is the electron-proton correlation potential. Note that the terms $\boldsymbol{J}^{\mathrm{ep}}(\boldsymbol{J}^{\mathrm{pe}})$ and $\boldsymbol{V}_c^{\mathrm{ep}}(\boldsymbol{V}_c^{\mathrm{pe}})$ explicitly depend on *both* the time-dependent electronic and the protonic densities, and therefore these multi-component contributions introduce strong coupling and vibronic effects.

By multiplying $\boldsymbol{C}^{\mathrm{e}\dagger}(t)\left(\boldsymbol{C}^{\mathrm{p}\dagger}(t)\right)$ to the right of the upper (lower) equations in Eq. (3), and subtracting its adjoint, we arrive at the multicomponent Von Neumann's equation,

$$\begin{aligned}
i\hbar\frac{\partial}{\partial t}\boldsymbol{P}^{\mathrm{e}}(t) &= [\boldsymbol{F}^{\mathrm{e}}(t,\boldsymbol{P}^{\mathrm{e}}(t),\boldsymbol{P}^{\mathrm{p}}(t)),\boldsymbol{P}^{\mathrm{e}}(t)] \\
i\hbar\frac{\partial}{\partial t}\boldsymbol{P}^{\mathrm{p}}(t) &= [\boldsymbol{F}^{\mathrm{p}}(t,\boldsymbol{P}^{\mathrm{p}}(t),\boldsymbol{P}^{\mathrm{e}}(t)),\boldsymbol{P}^{\mathrm{p}}(t)]
\end{aligned} \tag{7}$$

It is important to note that the differential equations for the electron and proton density matrices do not evolve independently and are coupled together. The electron density matrix contributes to the proton Fock matrix through the electron-proton Coulomb potential and the electron-proton correlation potential in NEO-DFT, and the proton density matrix contributes to the electron Fock matrix through these same terms. Therefore, these two equations need to be solved simultaneously. In this work, Eq. (7) is propagated in tandem with the modified midpoint unitary transformation (MMUT) algorithm (see the SI for more information),[40,41] giving rise to the real-time time-dependent NEO formalism (RT-NEO-TDHF and RT-NEO-TDDFT).

The electric-dipole approximation in length gauge to the field-matter operator is invoked to simulate an external electric field. Given the time-dependent electronic and protonic one-particle densities, the time-dependent electronic and nuclear dipole moments can be

computed as

$$D^{\mathrm{e}}_{\gamma}(t) = \mathrm{Tr}[\boldsymbol{P}'^{\mathrm{e}}(t) \cdot \boldsymbol{d}'^{\mathrm{e}}_{\gamma}] \tag{8}$$

$$D^{\mathrm{p}}_{\gamma}(t) = \mathrm{Tr}[\boldsymbol{P}'^{\mathrm{p}}(t) \cdot \boldsymbol{d}'^{\mathrm{p}}_{\gamma}] \tag{9}$$

where $\gamma \in \{x, y, z\}$ and $d^{\mathrm{e(p)}}_{\gamma,\mu\nu} = \langle \mu^{\mathrm{e(p)}} | r_{\gamma} | \nu^{\mathrm{e(p)}} \rangle$. Electronic (protonic) basis functions are denoted as $\mu^{\mathrm{e(p)}}$. The absorption cross section is computed as $\sigma(\omega) \propto \omega \sum_{i=x,y,z} \mathrm{Im}[\tilde{D}_i(\omega)]$, in which $\tilde{D}_i(\omega)$ is the Fourier transform of the time-dependent electron/proton dipole moment.

The RT-NEO-TDHF and RT-NEO-TDDFT algorithms and quantum dynamics are implemented in the Chronus Quantum open source package.[42] LR-NEO-TDHF and LR-NEO-TDDFT calculations were performed with a developer's version of Q-Chem,[43] which will be available in the Q-Chem 5.3 release. The B3LYP[44–46] functional was used in the DFT calculations, and the epc17-2 functional[34] was used to include the electron-proton correlation effects (see SI for additional computational details).

We first apply the RT-NEO-TDHF and RT-NEO-TDDFT methods to predict molecular spectra. The two test systems we choose are the FHF^- and HCN molecules. In these benchmark tests, only protons in addition to electrons are treated quantum mechanically, while the rest of the nuclei are frozen. Three quantum dynamical simulations were carried out, starting from the converged ground state NEO-HF or NEO-DFT wavefunction perturbed with three delta electric fields at $t = 0$ for the duration of one time-step with amplitude 1 mHartree/Å, polarized in the x, y, and z directions.

The time-evolutions of the electronic and protonic dipole moments of FHF^- obtained with the RT-NEO-TDDFT approach are plotted in Fig. 1. Both the electronic and the protonic dipole moments can be seen to oscillate around their equilibrium values. As protons are much heavier than electrons, the protonic vibrational frequency is much lower than that of the electrons. A closer look reveals that the proton dipole moment contains high-frequency components modulated by the oscillations of the electronic dipole moment, as shown in the

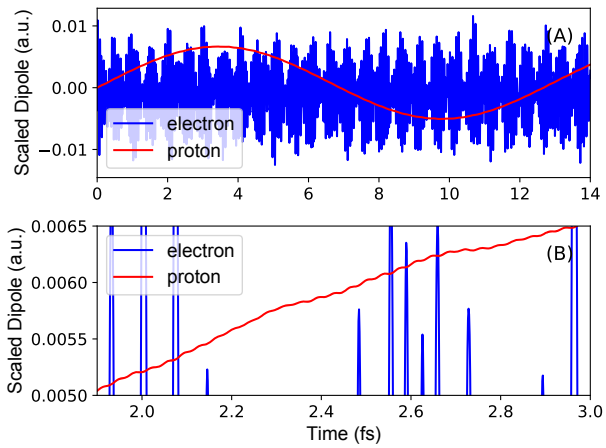

Figure 1: Electron and proton dipole moment evolution of RT-NEO-TDDFT for FHF^- for time from 0∼14 fs(**A**) and 1.9∼3 fs(**B**). Dipole moments are scaled by 10000 and 100 for protons and electrons respectively.

bottom part of Fig. 1. These observations show direct evidence that the proton density responds to the change in electron density due to vibronic coupling.

The time evolutions of the total dipole moments of the HCN molecule predicted by the RT-NEO-TDDFT and RT-TDDFT[3,47] methods are compared in Fig. 2. It is worth noting that since the proton dipole fluctuations are much smaller than those of the electrons, the total dipole moment is dominated by the electronic component. In the short-time regime, the inclusion of proton motion does not change the dynamics of the total dipole moment significantly because the proton density change is negligible at short times. However, at longer propagation times, the total dipole moment obtained with RT-NEO-TDDFT yields noticeable differences compared to that from RT-TDDFT with a frozen proton, both in terms of frequencies and intensities. This again is due to the presence of electron-proton vibronic coupling.

The time-dependent protonic dipole moment gives rise to vibrational signatures associated with the protonic degrees of freedom. The predicted proton vibrational spectra are plotted in Fig. 3 for HCN and FHF^-. For linear molecules such as HCN and FHF^-, there are four vibrational modes in total, but only three modes are active when the heavy nuclei are fixed. Furthermore, two among the three visible modes are degenerate, leading to only two

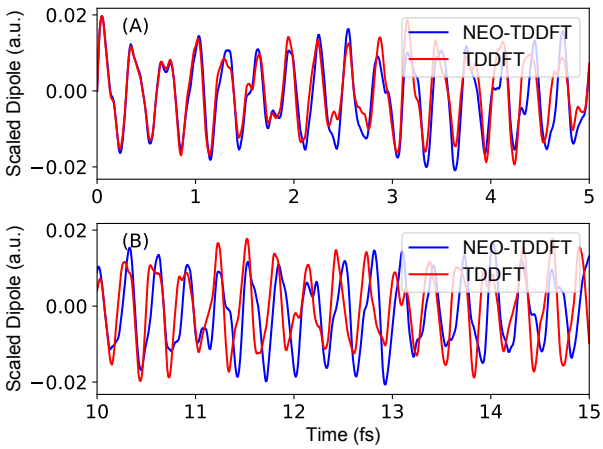

Figure 2: Comparison of the total dipole moment evolution between RT-NEO-TDDFT and RT-TDDFT for HCN molecule for short time duration (**A**) and long time duration (**B**).

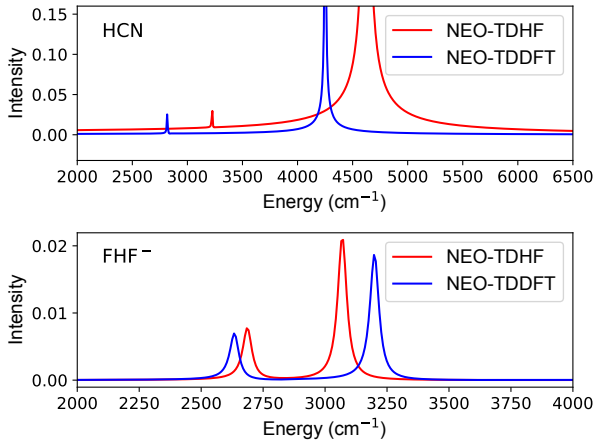

Figure 3: Calculated vibrational spectra of HCN (**Top**) and FHF^- (**Bottom**) with RT-NEO-TDHF and RT-NEO-TDDFT .

distinct peaks in the spectrum. The peak positioned at higher energy arises from the stretching motion of the C-H and F-H bonds, and the other low-frequency peak corresponds to the degenerate pair of bending motions. In general, the vibrational frequencies predicted by RT-NEO-TDDFT are shifted by a few hundred cm^{-1} compared to those predicted by RT-NEO-TDHF. Although the results agree with corresponding linear response calculations, there is no uniform trend of the direction of shifting observed in the test systems. These differences can be attributed to the more accurate description of coupled electron-proton quantum dynamics provided by the electron-proton correlation functional in NEO-DFT.[34]

At the asymptotic weak perturbation limit, spectra obtained from real-time simulations and linear response calculations should converge,[40] and this is indeed the case, as indicated by the comparison to results obtained with LR-TDHF and LR-TDDFT with the same basis sets and functionals. It is also worth noting that the proton vibrational frequencies are sensitive to both the electronic and nuclear basis sets. Increasing the size of the electronic and nuclear basis sets for the quantum proton has been shown to significantly lower the hydrogen bending frequency in HCN (see SI).[38,48] The LR-TDDFT method has been benchmarked against a numerically accurate grid-based method,[48] suggesting that the basis sets used in the current work are sufficient for qualitative agreement and, at the same time, allow for a clear interpretation of the computed spectra.

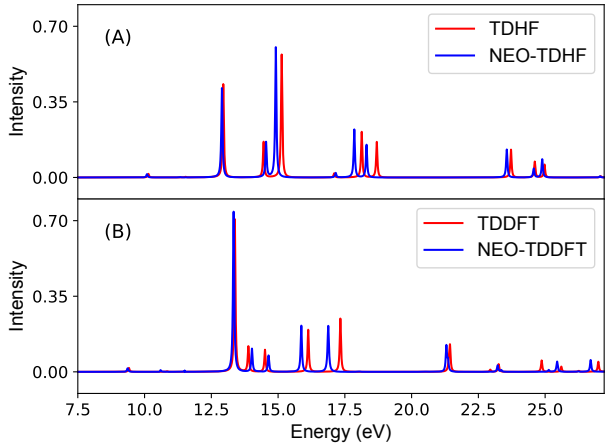

Figure 4: Calculated electronic spectra of the HCN molecule: (**A**) RT-NEO-TDHF and RT-TDHF, and (**B**) RT-NEO-TDDFT and RT-TDDFT.

We now examine how nuclear quantum effects are manifested in the electronic spectrum. The predicted electronic spectra are plotted in Fig. 4 for HCN and Fig. 5 for FHF^-. In both molecules, nuclear quantum effects modify the electronic spectrum in terms of both peak position (excitation energy) and peak intensity (oscillator strength). The non-Born-Oppenheimer vibronic mixing in the NEO approach gives rise to mixings of the electronic and protonic excitations and changes in transition densities, which result in changes in the excitation energies and oscillator strengths.

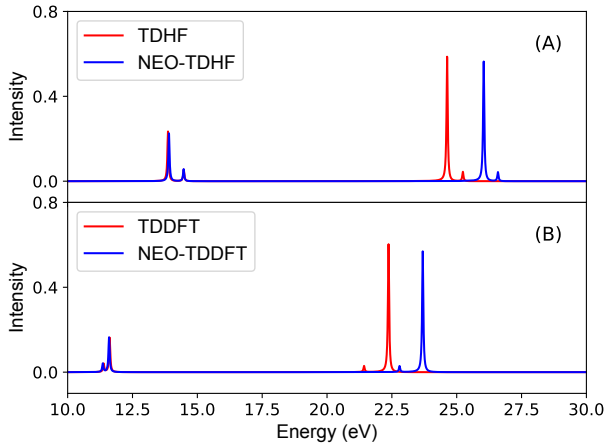

Figure 5: Calculated electronic spectra of FHF^- molecule: (**A**) RT-NEO-TDHF and RT-TDHF, and (**B**) RT-NEO-TDDFT and RT-TDDFT.

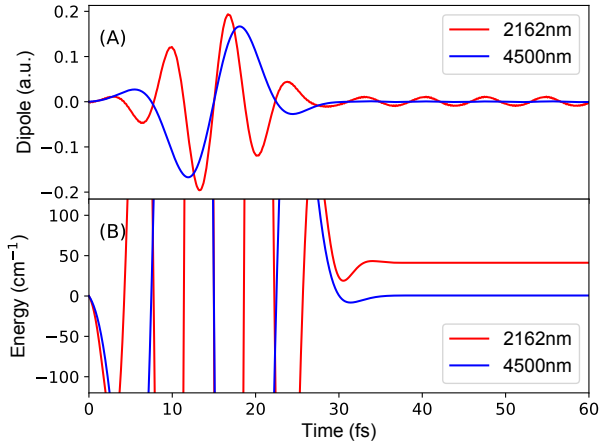

Figure 6: Total dipole (**A**) and energy (**B**) dynamics driven by laser fields with wavelengths of 2162 and 4500 nm.

The lower electronic excitation energies are mostly unchanged, whereas higher energy excitations seem to be more affected by protonic quantum effects, as observed previously with the linear response NEO-TDDFT approach.[38,48] This observation suggests that the electron-proton vibronic coupling becomes more important for the description of non-Born-Oppenheimer surfaces of higher-energy excited states. In addition to shifting the peak positions, nuclear quantum effects also slightly modify the peak intensity arising from variations in the transition densities.

The discussion above illustrates the fundamental characteristics of the RT-NEO approach

from the perspective of linear absorption spectra. However, the unique strength of this approach lies in its capability to resolve ultrafast nonequilibrium chemical processes. For the first example, we investigate the ultrafast vibrational excitation driven by an electric field pulse, *i.e.*, time-resolved infrared spectroscopy. Two different ∼30 fs laser pulses with 2162 nm and 4500 nm wavelengths are applied to drive the quantum dynamics of HCN (see Fig. 6). The laser field is modelled using a sine function with a Gaussian envelope (see SI for details) and a maximum amplitude of 0.01 a.u. polarized along the bond axis.

The fundamental vibrational frequency of the CH stretching mode is predicted by RT-NEO-TDHF to be 2162 nm. When the driving field is off-resonant, the protonic dipole moment follows the field adiabatically. When the field is turned off, the system exhibits negligible energy absorption and much smaller proton dipole moment oscillations that are not visible in Fig. 6. In contrast, when a resonant driving field is used, we observe a noticeable amount of energy absorption after the laser is turned off, and the proton dipole moment exhibits significant oscillations, as shown in Fig. 6. This test demonstrates that the RT-NEO approach can be conveniently used to simulate time-resolved vibrational spectroscopy.

For the second example, we use RT-NEO-TDDFT to simulate the excited state intramolecular proton transfer (ESIPT) in o-hydroxybenzaldehyde (oHBA). The ESIPT in oHBA has been studied extensively with both theoretical[49,50] and spectroscopic[51] techniques. The potential energy surface predicted by TDDFT and coupled cluster methods show that the proton transfer occurs without any energy barrier on the S_1 ($\pi\pi^*$) excited state. This finding is corroborated by time-resolved photoelectron spectroscopy, which demonstrated that the proton transfer occurs in 50 fs.[51] The initial condition for the quantum dynamical simulations herein is prepared to simulate the vertical photoabsorption at $t = 0$. The excited electronic state is modelled by an electronic transition from the highest occupied molecular orbital (HOMO) to the electronic lowest unoccupied molecular orbital (LUMO), which gives rise to an $S_0 \rightarrow S_1$ excitation. In order to provide the dynamical flexibility to allow the proton to transfer on the excited state, two sets of nuclear and electronic basis functions are

associated with the transferring hydrogen, with one set centered near the donor oxygen (O_D) and the other centered near the acceptor oxygen (O_A) (see SI for computational details).

Two geometries are considered in the simulations: the ground state minimum energy structure and the restricted excited state structure. The restricted excited state geometry was obtained by optimizing the geometry on the excited state surface but fixing the H-O_D distance to the ground state value. Such a structure was used by Aquino *et al*[50] to investigate the importance of excited state structural relaxation on the proton transfer dynamics. The resulting structures show an O_D-O_A distance of 2.64 Å for the ground state geometry and 2.51 Å for the restricted excited state geometry. For both geometries, three proton basis function centers were utilized to enable the proton to transfer from the donor to the acceptor oxygen (see SI for more details).

The H-O_D and H-O_A distances obtained from the quantum dynamical simulations are plotted in Fig. 7. Electronic vertical excitation gives rise to a nonequilibrium proton motion, as seen in Fig. 7A. When the molecular backbone is frozen at the ground state geometry, only the bound H-O_D vibration can be observed, where the the H-O_D distance changes by up to +3% of the ground state equilibrium distance (Fig. 7A). Thus, in the absence of excited state structural relaxation, proton transfer in oHBA is not a spontaneous process. As demonstrated by a previous study,[50] proton transfer is a multi-dimensional process with strong couplings between the transferring proton and other internal coordinates. Using the restricted excited state geometry as the initial condition, an ultrafast spontaneous proton transfer event is observed on the S_1 state (Fig. 7B). Note that the observed reaction time of ∼8 fs does not include the time for the molecular geometry to relax on the excited state. This test showcases the capabilities of RT-NEO approaches for resolving excited state quantum dynamics and illustrates the importance of structural relaxation effects in excited state proton transfer. Moreover, a movie (**link to WEO**) illustrating the time-dependent nonequilibrium density changes for the electrons and the quantum proton following photoexcitation highlights the intricate coupling between the electronic and nuclear quantum dynamics.

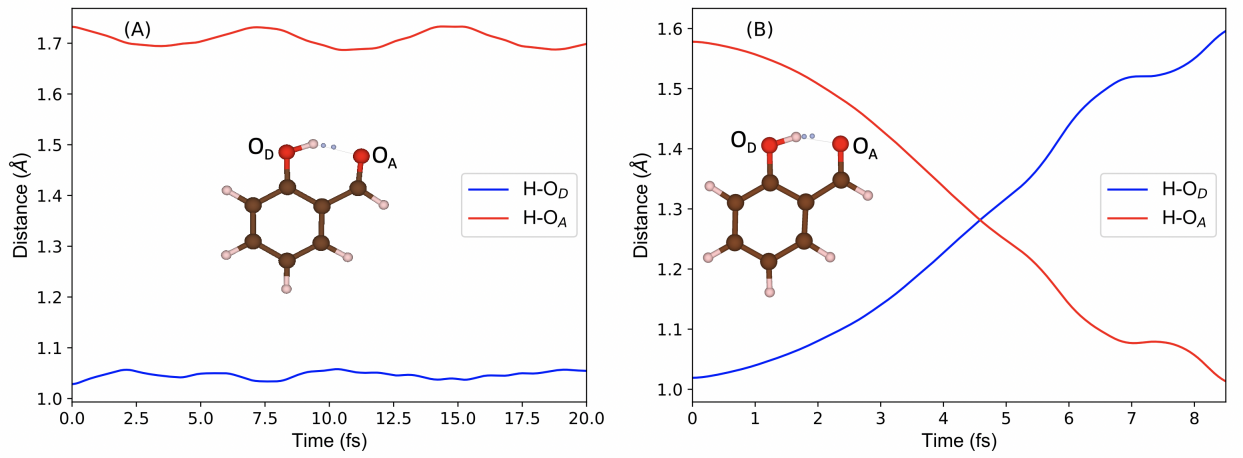

Figure 7: Distance from the transferring proton to the donor oxygen (O_D) and the acceptor oxygen (O_A) as a function of time for the ESIPT system with the optimized ground state structure (**A**) and the restricted optimized excited state structure (**B**).

This Letter presents the development of a new approach for simulating quantum dynamics that integrates the nuclear and electronic dynamics described by time-dependent Hartree-Fock or density functional theory within the nuclear-electronic orbital framework. We have demonstrated that RT-NEO is a powerful method that can resolve spectroscopic and dynamical properties of quantum mechanically coupled electrons and nuclei. Most importantly, this work lays the theoretical foundation of RT-NEO based quantum dynamical tools for simulating time-resolved nonlinear spectroscopies and nonadiabatic quantum dynamics.

Acknowledgement

The development of quantum dynamics for studies of proton transfer was supported by IDREAM (Interfacial Dynamics in Radioactive Environments and Materials), an Energy Frontier Research Center funded by the U.S. Department of Energy (DOE), Office of Science, Basic Energy Sciences (BES). The development of the Chronus Quantum open source software package is supported by the National Science Foundation (OAC-1663636). The development of the real-time electronic structure method is funded by the US Department

of Energy (DE-SC0006863). The development of nuclear-electronic orbital time-dependent density functional theory methods is supported by the National Science Foundation Grant No. CHE-1762018. Computations were facilitated through the use of advanced computational, storage, and networking infrastructure provided by the Hyak supercomputer system at the University of Washington, funded by the Student Technology Fee. L. Z. acknowledges the Dalton Postdoc Fellowship at the University of Washington for funding.

Supporting Information Available: The supporting information includes: computational details; detailed expressions for electron and proton Fock matrices; comparison of dipole dynamics with different time-steps; formulation of frequency-dependent laser field; numerical propagation schemes; comparison of excitation energies between LR-NEO and RT-NEO; LR-NEO-TDHF results on HCN with larger basis set; movie of ESIPT with restricted optimized excited state structure.

References

(1) Negele, J. W. The Mean-Field Theory of Nuclear Structure and Dynamics. *Rev. Mod. Phys.* **1982**, *54*, 913.

(2) Li, X.; Tully, J. C.; Schlegel, H. B.; Frisch, M. J. Ab Initio Ehrenfest Dynamics. *J. Chem. Phys.* **2005**, *123*, 084106.

(3) Isborn, C. M.; Li, X.; Tully, J. C. TDDFT Ehrenfest Dynamics: Collisions between Atomic Oxygen and Graphite Clusters. *J. Chem. Phys.* **2007**, *126*, 134307.

(4) Ding, F.; Goings, J. J.; Liu, H.; Lingerfelt, D. B.; Li, X. Ab Initio Two-Component Ehrenfest Dynamics. *J. Chem. Phys.* **2015**, *143*, 114105.

(5) Goings, J. J.; Lingerfelt, D. B.; Li, X. Can Quantized Vibrational Effects Be Obtained from Ehrenfest Mixed Quantum-Classical Dynamics? *J. Phys. Chem. Lett.* **2016**, *7*, 5193–5197.

(6) Andrade, X.; Castro, A.; Zueco, D.; Alonso, J. L.; Echenique, P.; Falceto, F.; Rubio, A. Modified Ehrenfest Formalism for Efficient Large-Scale ab initio Molecular Dynamics. *J. Chem. Theory Comput.* **2009**, *5*, 728–742.

(7) Tully, J. C. Trajectory Surface Hopping Approach to Nonadiabatic Molecular Collisions: The Reaction of H+ with D_2. *J. Chem. Phys.* **1971**, *55*, 562.

(8) Tully, J. C. Molecular Dynamics with Electronic Transitions. *J. Chem. Phys.* **1990**, *93*, 1061.

(9) Hammes-Schiffer, S.; Tully, J. C. Proton Transfer in Solution: Molecular Dynamics with Quantum Transitions. *J. Chem. Phys.* **1994**, *101*, 4657.

(10) Subotnik, J. E.; Jain, A.; Landry, B.; Petit, A.; Ouyang, W.; Bellonzi, N. Understanding the Surface Hopping View of Electronic Transitions and Decoherence. *Annu. Rev. Phys. Chem.* **2016**, *67*, 387–417.

(11) Wang, L.; Akimov, A.; Prezhdo, O. V. Recent Progresses in Surface Hopping: 2011-2015. *J. Phys. Chem. Lett.* **2016**, *7*, 2100–2112.

(12) Ben-Nun, M.; Quenneville, J.; Martínez, T. J. Ab Initio Multiple Spawning: Photochemistry from First Principles Quantum Molecular Dynamics. *J. Phys. Chem. A* **2000**, *104*, 5161–5175.

(13) Curchod, B. F. E.; Martínez, T. J. Ab Initio Nonadiabatic Quantum Molecular Dynamics. *Chem. Rev.* **2018**, *118*, 3305–3336.

(14) Mignolet, B.; Curchod, B. F. E. Excited-State Molecular Dynamics Triggered by Light Pulses-*Ab Initio* Multiple Spawning vs Trajectory Surface Hopping. *J. Phys. Chem. A* **2019**, *123*, 3582–3591.

(15) Mignolet, B.; Curchod, B. F. E. A Walk Through the Approximations of *ab initio* Multiple Spawning. *J. Chem. Phys.* **2018**, *148*, 134110.

(16) Beck, M. H.; Jaĕckle, A.; Worth, G. A.; Meyer, H.-D. The Multiconfiguration Time-Dependent Hartree (MCTDH) Method: A Highly Efficient Algorithm for Propagating Wavepackets. *Phys. Rev.* **2000**, *324*, 1–105.

(17) Wang, H.; Thoss, M. Multilayer Formulation of the Multiconfiguration Time-Dependent Hartree Theory. *J. Chem. Phys.* **2003**, *119*, 1289.

(18) Heller, E. J. Time-dependent Approach to Semiclassical Dynamics. *J. Chem. Phys.* **1975**, *62*, 1544.

(19) Heller, E. J. Guided Gaussian Wave Packets. *Acc. Chem. Res.* **2006**, *39*, 127–134.

(20) Huynh, M. H. V.; Meyer, T. J. Proton-Coupled Electron Transfer. *Chem. Rev.* **2007**, *107*, 5004–5064.

(21) Hammes-Schiffer, S. Proton-Coupled Electron Transfer: Moving Together and Charging Forward. *J. Am. Chem. Soc.* **2015**, *137*, 8860–8871.

(22) Tamura, H.; Huix-Rotllant, M.; Burghardt, I.; Olivier, Y.; Beljonne, D. First-Principle Quantum Dynamics of Singlet Fission: Coherent versus Thermally Activated Mechanisms Governed by Molecular π Stacking. *Phys. Rev. Lett.* **2015**, *115*, 107401.

(23) Miyata, K.; Kurashige, Y.; Watanabe, K.; Sugimoto, T.; Takahashi, S.; Tanaka, S.; Takeya, J.; Yanai, T.; Matsumoto, Y. Coherent Singlet Fission Activated by Symmetry Breaking. *Nat. Chem.* **2017**, *9*, 983–989.

(24) Walters, P. L.; Makri, N. Quantum-Classical Path Integral Simulation of Ferrocene-Ferrocenium Charge Transfer in Liquid Hexane. *J. Phys. Chem. Lett.* **2015**, *6*, 4959–4965.

(25) Vacher, M.; Bearpark, M. J.; Robb, M. A.; Malhado, J. P. Electron Dynamics upon Ionization of Polyatomic Molecules: Coupling to Quantum Nuclear Motion and Decoherence Morgane. *Phys. Rev. Lett.* **2017**, *118*, 083001.

(26) Wang, Q.; Domen, K. Particulate Photocatalysts for Light-Driven Water Splitting: Mechanisms, Challenges, and Design Strategies. *Chem. Rev.* **2019**, *Article ASAP*.

(27) Scholes, G. D.; Fleming, G. R.; Olaya-Castro, A.; van Grondelle, R. Lessons from Nature about Solar Light Harvesting. *Nat. Chem.* **2011**, *3*, 763–774.

(28) Seo, H.; Falk, A. L.; Klimov, P. V.; Miao, K. C.; Galli, G.; Awschalom, D. D. Quantum Decoherence Dynamics of Divacancy Spins in Silicon Carbide. *Nat. Commun.* **2016**, *7*, 12935.

(29) Webb, S. P.; Iordanov, T.; Hammes-Schiffer, S. Multiconfigurational Nuclear-Electronic Orbital Approach: Incorporation of Nuclear Quantum Effects in Electronic Structure Calculations. *J. Chem. Phys.* **2002**, *117*, 4106.

(30) Pak, M. V.; Hammes-Schiffer, S. Electron-Proton Correlation for Hydrogen Tunneling Systems. *Phys. Rev. Lett.* **2004**, *92*, 103002.

(31) Swalina, C.; Pak, M. V.; Chakraborty, A.; ; Hammes-Schiffer, S. Explicit Dynamical Electron-Proton Correlation in the Nuclear-Electronic Orbital Framework. *J. Phys. Chem. A* **2006**, *110*, 9983–9987.

(32) Chakraborty, A.; Pak, M. V.; Hammes-Schiffer, S. Development of Electron-Proton Density Functionals for Multicomponent Density Functional Theory. *Phys. Rev. Lett.* **2008**, *101*, 153001.

(33) Yang, Y.; Brorsen, K. R.; Culpitt, T.; Pak, M. V.; Hammes-Schiffer, S. Development of a Practical Multicomponent Density Functional for Electron-Proton Correlation to Produce Accurate Proton Densities. *J. Chem. Phys.* **2017**, *147*, 114113.

(34) Brorsen, K. R.; Yang, Y.; Hammes-Schiffer, S. Multicomponent Density Functional Theory: Impact of Nuclear Quantum Effects on Proton Affinities and Geometries. *J. Phys. Chem. Lett.* **2017**, *8*, 3488–3493.

(35) Swalina, C.; Pak, M. V.; Hammes-Schiffer, S. Alternative Formulation of Many-Body Perturbation Theory for Electron-Proton Correlation. *Chem. Phys. Lett.* **2005**, *404*, 394–399.

(36) Pavošević, F.; Culpitt, T.; Hammes-Schiffer, S. Multicomponent Coupled Cluster Singles and Doubles Theory within the Nuclear-Electronic Orbital Framework. *J. Chem. Theory Comput.* **2019**, *15*, 338–347.

(37) Pavošević, F.; Hammes-Schiffer, S. Multicomponent Equation-of-Motion Coupled Cluster Singles and Doubles: Theory and Calculation of Excitation Energies for Positronium Hydride. *J. Chem. Phys.* **2019**, *150*, 161102.

(38) Yang, Y.; Culpitt, T.; Hammes-Schiffer, S. Multicomponent Time-Dependent Density Functional Theory: Proton and Electron Excitation Energies. *J. Phys. Chem. Lett.* **2018**, *9*, 1765–1770.

(39) Li, X.; Millam, J. M.; Scuseria, G. E.; Frisch, M. J.; Schlegel, H. B. Density Matrix Search Using Direct Inversion in the Iterative Subspace as a Linear Scaling Alternative to Diagonalization in Electronic Structure Calculations. *J. Chem. Phys.* **2003**, *119*, 7651.

(40) Goings, J. J.; Lestrange, P. J.; Li, X. Real-Time Time-Dependent Electronic Structure Theory. *Wiley Interdiscip. Rev. Comput. Mol. Sci.* **2018**, *8*, e1341.

(41) Li, X.; Smith, S. M.; Markevitch, A. N.; Romanov, D. A.; Levis, R. J.; Schlegel, H. B. A Time-Dependent Hartree-Fock Approach for Studying the Electronic Optical Response of Molecules in Intense Fields. *Phys. Chem. Chem. Phys.* **2005**, *7*, 233–239.

(42) Williams-Young, D. B.; Petrone, A.; Sun, S.; Stetina, T. F.; Lestrange, P.; Hoyer, C. E.; Nascimento, D. R.; Koulias, L.; Wildman, A.; Kasper, J. et al. The Chronus Quantum Software Package. *Wiley Interdiscip. Rev. Comput. Mol. Sci.* **2019**, *e1436*.

(43) Shao, Y.; Gan, Z.; Epifanovsky, E.; Gilbert, A. T.; Wormit, M.; Kussmann, J.; Lange, A. W.; Behn, A.; Deng, J.; Feng, X. et al. Advances in Molecular Quantum Chemistry Contained in the Q-Chem 4 Program Package. *Mol. Phys.* **2015**, *113*, 184–215.

(44) Lee, C.; Yang, W.; Parr, R. G. Development of the Colle-Salvetti Correlation-Energy Formula into a Functional of the Electron Density. *Phys. Rev. B* **1988**, *37*, 785.

(45) Becke, A. D. Density-Functional Exchange-Energy Approximation with Correct Asymptotic Behavior. *Phys. Rev. A* **1988**, *38*, 3098.

(46) Becke, A. D. A New Inhomogeneity Parameter in Density-Functional Theory. *J. Chem. Phys.* **1998**, *109*, 2092.

(47) Li, X.; Tully, J. C. Ab Initio Time-Resolved Density Functional Theory for Lifetimes of Excited Adsorbate States at Metal Surfaces. *Chem. Phys. Lett.* **2007**, *439*, 199–203.

(48) Culpitt, T.; Yang, Y.; Pavošević, F.; Tao, Z.; Hammes-Schiffer, S. Enhancing the Applicability of Multicomponent Time-Dependent Density Functional Theory. *J. Chem. Phys.* **2019**, *150*, 201101.

(49) Scheiner, S. Theoretical Studies of Excited State Proton Transfer in Small Model Systems. *J. Phys. Chem. A* **2000**, *104*, 5898–5909.

(50) Aquino, A. J. A.; Lischka, H.; Hättig, C. Excited-State Intramolecular Proton Transfer: A Survey of TDDFT and RI-CC2 Excited-State Potential Energy Surfaces. *J. Phys. Chem. A* **2005**, *109*, 3201–3208.

(51) Lochbrunner, S.; Schultz, T.; Schmitt, M.; Shaffer, J. P.; Zgierski, M. Z.; Stolow, A. Dynamics of Excited-State Proton Transfer Systems via Time-Resolved Photoelectron Spectroscopy. *J. Chem. Phys.* **2001**, *114*, 2519.